Int. J. Electrochem. Sci., 16 **(2021)** Article Number: 211234, doi: 10.20964/2021.12.25

International Journal of
ELECTROCHEMICAL
SCIENCE
www.electrochemsci.org

Preparation and Corrosion Resistance of Superhydrophobic Ni-P-Al_2O_3 Coating on Pipeline Steel in simulated alkaline soil solution

Qiuli Zhang[*], *Ziyue Song, Zhaoyang Chen, Yi Feng, Pei Zhang, Jun Zhou*

School of Chemistry and Chemical Engineering, Xi'an University of Architecture and Technology, Xi'an, China
[*]E-mail: qiulizhang@126.com

Received: 1 September 2021 / *Accepted:* 9 October 2021 / *Published:* 10 November 2021

Superhydrophobic coating with good corrosion resistance has become a research hotspot. The nano-Ni-P-Al_2O_3 composite coating was prepared on the surface of pipeline steel by electrodeposition technology with nano-Al_2O_3 particles into the bath, which aimed to reduce the corrosion of pipeline steel in the alkaline soil environment. The micromorphologies, hydrophobicity, and corrosion resistance of the electrodeposited composite coatings at different concentrations of nano-Al_2O_3 (0, 5, 10, and 15 g/L) were studied by scanning electron microscope (SEM), energy disperse spectroscopy-mapping (EDS-mapping), contact angle, and electrochemical measurements. The papillary protrudes grew on the surface of the coating with the increase of the nano-Al_2O_3 content. The coating surface was uniform and compact when the nano-Al_2O_3 particle concentration was 15 g/L. The nano-Ni-P-Al_2O_3 composite coating was superhydrophobic, and the maximum contact Angle was 158.3°. The electrochemical test results showed that the shape characteristics of EIS and potentiodynamic polarization curve of the coating were not changed by the content of nano-Al_2O_3. With the increase of the nano-Al_2O_3 concentration, the capacitive arc radius and E_{corr} of the composite coating increased, while I_{corr} decreased, which indicated that the corrosion resistance of the composite coating in the simulated soil solution was gradually enhanced. The coating with 15 g/L nano-Al_2O_3 particles had the best corrosion resistance, and the corrosion rate was significantly lower than that of X100 pipeline steel.

Keywords: Superhydrophobic, nano-Al_2O_3, composite coating, corrosion resistance

1. INTRODUCTION

Pipeline steel is a kind of hot-rolled plate and strip used in natural gas transportation, oil development pipeline, and container, which is widely applied in industrial production [1]. Pipeline steels are used in the soil environment for a long time, which is affected by the internal and external working environment and production conditions, resulting in its corrosion and degradation [2]. Due to the high

surface energy of the pipeline steel, the water-based mixture in the soil environment is easy to spread on its surface, which increases the contact between water (and/or other corrosive substances) and pipeline steel surface, thus increasing the possibility of corrosion. Moreover, the adhesion between the water-based mixture and pipe wall leads to scaling on the pipe wall, which not only seriously affects the service life of pipeline steel, but also leads to equipment damage, resource waste, and huge economic losses [3-6]. Therefore, it is necessary to take effective measures on the surface of the pipeline steel by reducing the contact area of the two-phase interface [7].

At present, the superhydrophobic surface (surface with water contact angle greater than 150° and rolling angle less than 10°) with unique water repellency and non-wetting properties is widely used in corrosion protection of metals, such as self-cleaning, hydrophobic antifouling, drag, and friction reduction [8-11]. There are two conditions to construct a superhydrophobic surface on the solid surface: 1) the solid surface has low surface energy; 2) the solid surface has a certain micro-nano roughness. Therefore, the superhydrophobic surfaces are prepared with the help of low surface energy materials and micro-nano rough structures [12]. Appropriate surface morphologies play a decisive role in obtaining superhydrophobic properties [13]. Up to now, many researchers successfully prepared superhydrophobic surfaces by sol-gel method [14], anodic oxidation method [15], plasma etching [16], template [17], 3D printing [18], and electrodeposition [19]. However, most of the above methods are complex, time-consuming, expensive, or limited in application scenarios. In contrast, the electrodeposition technology has the advantages of the simple preparation process, strong controllability of micromorphology, and low cost, which can be effectively applied to the construction of superhydrophobic surfaces [20].

The anticorrosion coatings are mostly single nickel coating in the previous studies, which is difficult to meet the actual requirements of industrial production [12]. The corrosion resistance and hardness of the binary or multicomponent alloy coatings are higher than that of the single nickel coatings [21-23]. In recent years, various composite coatings prepared by electrodeposition technology are widely used in people's life and production because of their excellent properties. Hard ceramic particles (such as Al_2O_3, SiC, TiO_2, and Si_3N_4) and rare earth oxides (such as CeO_2 and La_2O_3) served as second-phase reinforcement particles for research [21, 24-30]. Fei Cai et al. [31] prepared pure nickel, Ni-Co, and Ni-Co-Al coatings by electrodeposition method, and found that Al particles reduced the grain size of the coatings and enhanced the corrosion resistance of the coatings. Sumit chhangani [32] prepared Ni-Al coating on the titanium plate by pulse electrodeposition, and studied the effects of different Al content on the grain structure and tensile strength of the coating. The results showed that the tensile strength of the coating increased first and then decreased with the increase of the Al content. R. R. oberle et al. [33] prepared nano-composite Ni-Al_2O_3 coating by electrodeposition method, which had better physical properties and higher hardness, thermal conductivity, and electrical conductivity than pure nickel coating. The existing studies found that the Ni-Al_2O_3 composite coating prepared by co-deposition technology (SCD) had excellent corrosion resistance due to the presence of Al_2O_3 on the surface of the coating [34, 35].

The alkaline saline soil in the west of China is one of the most typical and most corrosive soil types in China, which is widely distributed and rich in chloride, sulfate, and carbonate, causing great corrosion damage to pipeline steel. However, the corrosion research of pipeline steels mainly focused on the acidic and neutral environment, while the corrosion of pipeline steels in the alkaline soil is less.

Herein, nano Ni-P-Al_2O_3 composite coating was prepared on the surface of X100 pipeline steel by electrodeposition technology after adding nano-Al_2O_3 into the bath. The coating exhibited superhydrophobicity after modification with the stearic acid solution. The microstructure and hydrophobic properties of the composite coatings with different nano-Al_2O_3 contents (0, 5, 10, and 15 g/L) were studied, and the influence of different coatings on the corrosion resistance of X100 pipeline steel in the alkaline soil environment was analyzed, which provided data reference for the corrosion resistance of X100 pipeline steel.

2. MATERIALS AND METHODS

2.1 Materials

The chemical composition of X100 pipeline steel (as the cathode) used in the electrodeposition process is shown in Table 1. Pure nickel plate worked as the anode, and its chemical composition is shown in Table 2. Compared with Al micro-particles, Al nanoparticles significantly increased the number of particles per unit volume of the coating and reduced the grain size [35]. The particle size of Al_2O_3 used in this study is about 30 nm (Rhawn, 30nm-α-Al_2O_3,100 g).

Table 1. Chemical composition of X100 pipeline steel in wt.% of the material.

Element	C	Si	Mn	Ni	Cr	Mo	Ti+Nb	Fe
X100 pipeline steel	0.06-0.1	0.2-0.5	1.0-3.0	0.3-0.4	0.03-0.05	0.2-0.4	<0.2	bal

Table 2. Chemical composition of pure nickel plate in wt.% of the material.

Element	Fe	Mn	Si	P	Cu	Mg	C	Ni
pure nickel plate	<0.01	<0.002	<0.01	0.0003	<0.01	<0.001	0.002	bal

2.2 Preparation of electrodes

The X100 pipeline steel was machined into 8 mm × 8 mm × 3 mm, the working area was 0.64 cm2. The steel was welded to the copper wire and then wrapped with epoxy resin. The working surface was ground with SiC papers of #240 to #1500, followed by rinsing with acetone and deionized water. Finally, the electrode was wiped with anhydrous ethanol, and dried for standby. The pure nickel plate, with a size of 40 mm × 15 mm × 3 mm, was weld to the copper wire. The pure nickel plate was cleaned with deionized water before the experiment.

2.3 Design of the experiments

X100 pipeline steel was subjected to ultrasonic deoiling and sulfuric acid activation before electrodeposition. The solution used for ultrasonic oil removal was composed of NaOH (15 g/L), Na_2CO_3 (30 g/L), and $Na_3PO_4 \cdot 12H_2O$ (20 g/L). The ultrasonic time was 25 min. The activation step used 0.5 mol/L of H_2SO_4, and the activation time was 120 s. The sample was cleaned with ultra-pure water after oil removal and activation.

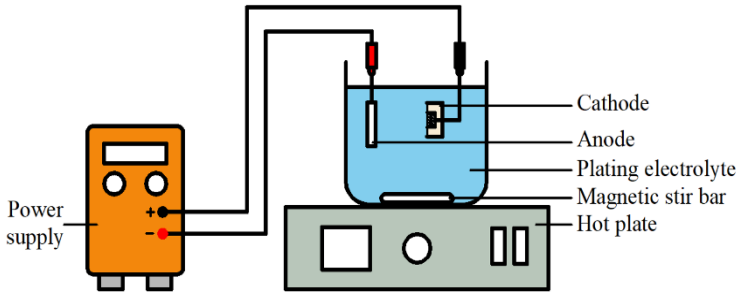

Figure 1. Schematic diagram of electrodeposition.

Fig. 1 shows a schematic diagram of the electrodeposition process. In the electrodeposition process, the cathode was X100 pipeline steel, the anode was pure nickel plate, the electrodeposition temperature was 50 ℃, and the time was 120 min. The electrolyte used for electrodeposition included 150 g/L of $NiSO_4 \cdot 6H_2O$, 30 g/L of $NiCl_2 \cdot 6H_2O$, 20 g/L of H_3PO_3,30 g/L of H_3BO_3, 70 g/L of Citric acid, 0.1 g/L of Sodium dodecylbenzene sulfonate (SDBS, Sodium dodecylbenzene sulfonate), 25 g/L of NH_4Cl, 20 g/L of Sodium hypophosphite and 0.02 g/L of Thiourea, and nano-Al_2O_3. The bath was prepared in a beaker (1 L), and all reagents used were ACS grade. The electrolyte was continuously stirred at 300 rpm with a magnetic agitator to disperse Al_2O_3 particles evenly in the solution.

The sample was washed with deionized water after deposition, and then modified with a low surface energy solution. Most of the reported superhydrophobic surfaces were modified by fluorocarbon compounds, which are expensive, highly toxic, and highly bioaccumulative [36]. Therefore, the environmental-friendly, low-cost, and high-benefit non-fluorinated stearic acid (STA) [37] was selected for modification in the experiment. The modified solution with low surface energy was ethanol solution containing 1wt.% stearic acid, and the modification time was 60 min. After modification, the sample was dried in an oven at 100 ℃ for 90 min. After that, the prepared Ni-P-Al_2O_3 composite coatings were tested by SEM, EDS-Mapping, contact angle, and electrochemistry.

2.4 Characterization

The surface morphologies of different composite coatings were observed by SEM (Hitachi SU8010, Japan), and element mapping scanning was performed in combination with FESEM. The static contact angle (CA) of the coatings was measured by contact angle measurement (Kruss DSA100, Germany) at room temperature using 5 μL deionized water droplets. The mean value and deviation of

the contact angle was obtained by measuring at least three different positions on each sample. CA was calculated by a circle fitting method.

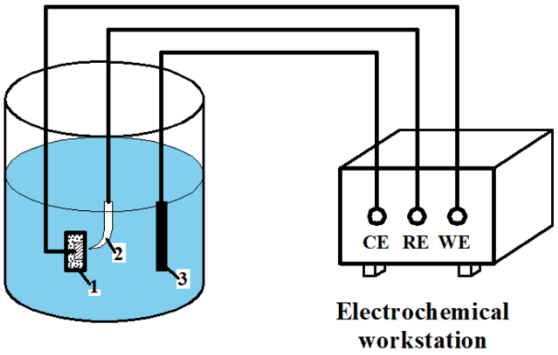

Figure 2. Scheme of electrochemical test. (1:X100 steel, 2: SCE, 3: High-purity graphite)

The electrochemical workstation (Correst CS2350, China) with a traditional three-electrode system was used to evaluate the corrosion resistance of the composite coatings in the simulated soil solutions, as shown in Fig. 2. The working electrode was the prepared X100 pipeline steel sample, the auxiliary electrode was the large-area high-purity graphite electrode, and the reference electrode was the saturated calomel electrode. All potentials in the paper were based on saturated calomel electrodes. The test solution was the alkaline simulated soil solution (0.2892 g/L $NaHCO_3$, 0.0813 g/L $CaCl_2$, 0.4315 g/L $MgSO_4 \cdot 7H_2O$, 5.6676 g/L Na_2SO_4, 0.0883 g/L Na_2CO_3, and 5% NaOH solution were used to adjust the pH of the solution to 10.0±0.1). Before the test, the sample was immersed in the solution for 1 hour until the system was stable and the open-circuit potential was measured. Under the following conditions (frequency range: 10^6Hz ~ 10^{-2}Hz, perturbation AC amplitude: 5 mV, logarithmic scan: 10 times, frequency: 10), 1 hour AC impedance spectrum at open circuit potential was obtained. The polarization curves were recorded at specific parameters (the potential range was -0.3 V ~ +0.6 V (vs. open circuit potential), and the scan rate was 0.5 mV/s). Cview analysis software was used to perform data fitting analysis on the potentiodynamic polarization curve, and Zsimpwin software was employed to fit the test data of electrochemical impedance spectroscopy.

3. RESULTS AND DISCUSSION

3.1 Microstructure of coatings on X100 Pipeline Steel with different nano-Al_2O_3 content

Fig. 3 shows the surface morphologies of the composite coatings with different nano-Al_2O_3 content. As shown in Fig. 3(a), the surface of Ni-P coating was basically uniform and flat, but there were fine pore defects. The papilla-like small protrusions began to form on the surface of the composite coating with the increase of nano-Al_2O_3 content. When nano-Al_2O_3 content was 5 g/L, the protrusions on the surface of the coating grew unevenly and had obvious defects. As shown in Fig. 3(c), when the

addition amount of nano-Al_2O_3 was 10 g/L, there were no obvious defects on the surface of the composite coating, and the surface protrusions increased continuously. As shown in Fig. 3(d), when nano-Al_2O_3 was 15 g/L, the surface of the coating was uniform and dense, and the grain size of the composite coating was obviously refined and smoother. Nanoparticles played a key role in the surface morphology of the coating. Therefore, the addition of nano-Al_2O_3 had a great influence on the formation of the micro-nano rough structure on the surface of the coating.

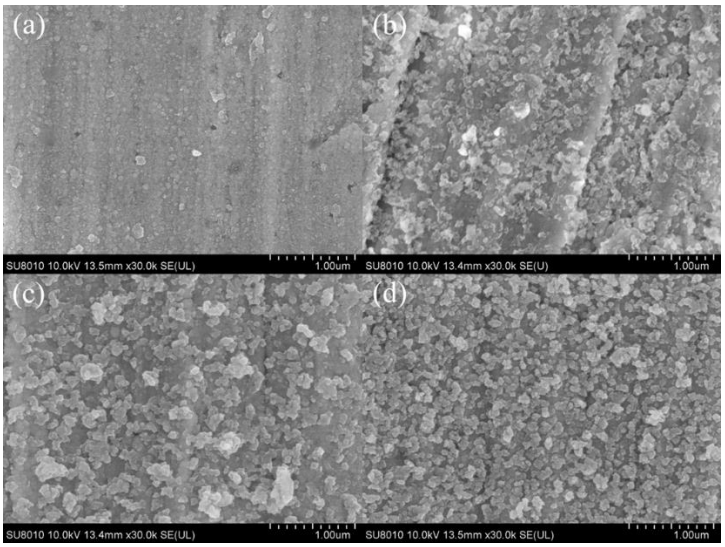

Figure 3. Surface morphologies of composite coatings deposited at (a) 0 g/L, (b) 5 g/L, (c) 10 g/L, and (d) 15 g/L nano-Al_2O_3.

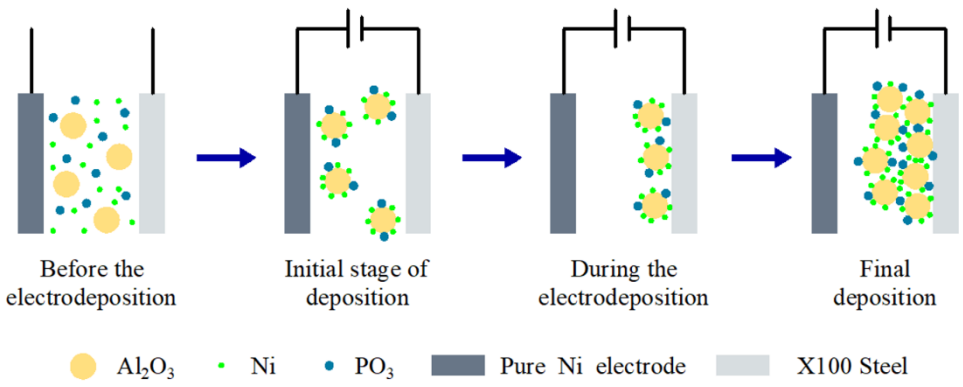

Figure 4. Electrodeposition mechanism of composite coating.

Many researches were carried out on the mechanism of the electro co-deposition, and several models were established, such as Guglielmi model [38], Celis model [39], and trajectory model [40]. In this study, the co-deposition behavior of the composite coating was described by the Guglielmi model, which included two successive adsorption steps. Fig. 4 shows the deposition mechanism of the composite coating. The particles in the solution were uniformly dispersed around the electrode by

mechanical stirring before deposition. At the beginning of the deposition, nano-Al_2O_3 particles were adsorbed by charged ions in the bath to form larger charged particles. Then, the charged particles arrived at the electrode surface through the action of the electric field. Currently, the adsorption force between the particles and the electrode surface was weak, resulting in the loose deposition of particles on the substrate of X100 pipeline steel. Deposition process, the charged particles entered the cathode surface by the electrophoresis attraction, the charged particles formed strong adsorption on the electrode surface to under the action of coulomb force, and the ions adsorbed on the nano-Al_2O_3 particles reduced. Due to the reduction of ions in the nano-Al_2O_3 particles, the combination of the nano-Al_2O_3 particles on the surface of the coating was assisted, and finally the nano-Al_2O_3 particles were embedded in the coating.

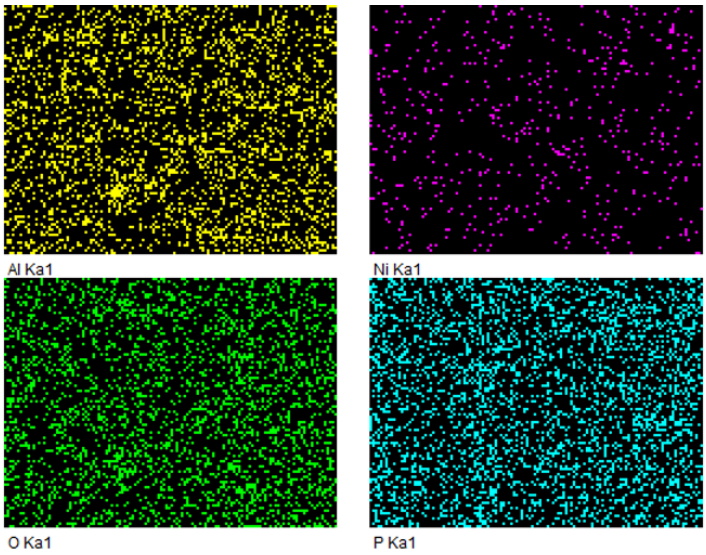

Figure 5. Element mapping of Ni-P-Al_2O_3 coating with 15g/L nano-Al_2O_3 particles.

As the concentration of nano-Al_2O_3 particles increased from 0 to 15 g/L, the uniform papillae grew on the coating surface, and the grain size decreased. There was a competition between the nucleation of nickel grains and crystal growth in the electrodeposition process [41, 42]. The nano-Al_2O_3 particles promoted the nucleation of new grains, which was due to the nucleation of Ni grains controlled by the second-phase nano-Al_2O_3 particles. The uniform co-deposition of the nano-Al_2O_3 particles reduced the competition between the nucleation and crystal growth of Ni grains, thus reducing the grain size of the coating. The elemental mapping scanning was carried out on the surface of the Ni-P-Al_2O_3 (15 g/L) coating to verify the uniform distribution of nano-Al_2O_3 particles, as shown in Fig. 5. The mapping results confirmed that Al, Ni, O, P, and other elements were distributed uniformly in the coating, that is, the distribution of the nano-Al_2O_3 particles in the composite Ni-P-Al_2O_3 coating was uniform.

3.2 Hydrophobicity of coatings on X100 Pipeline Steel with different nano-Al_2O_3 content

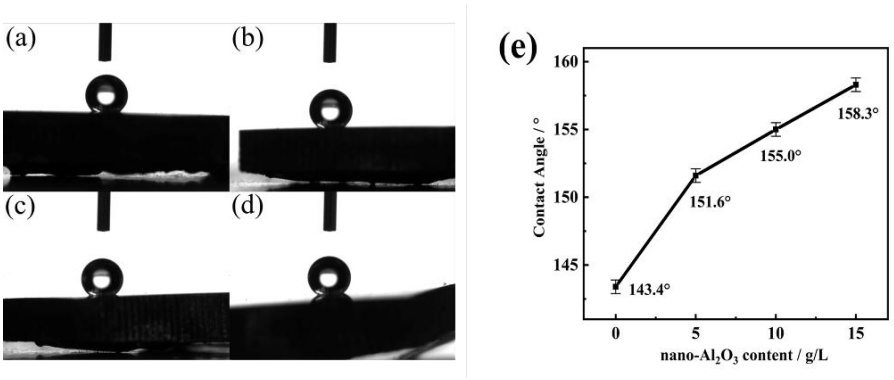

Figure 6. Contact angle of composite coatings deposited at (a) 0 g/L, (b) 5 g/L, (c) 10 g/L, and (d) 15 g/L nano-Al_2O_3; and (e) effect of the nano-Al_2O_3 content on the contact angle.

Fig. 6 shows the contact angle of the composite coating prepared with different nano-Al_2O_3 content. According to Wenzel theory, when the surface of the material is hydrophilic, the rougher the surface is, the better the hydrophilicity is, and the smaller the contact angle is. When the surface of the material is hydrophobic, the rougher the surface is, the better the hydrophobicity and the greater the contact angle is. The surface roughness is often affected by the surface topography, which is directly related to surface contact angle.

Figure 7. Screen capture of contact angle measurement of nano Ni-P-Al_2O_3 (15g/L) coating.

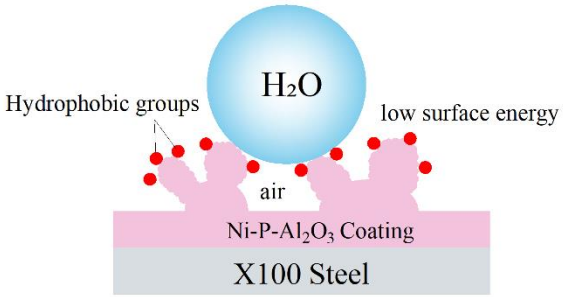

Figure 8. Superhydrophobic mechanism of composite coating.

All the coatings in this paper were modified by stearic acid, the surface energy of all coatings was the same, and the surface contact angle and adhesion were determined by the surface morphology. As can be seen from Fig. 6(e), the four prepared composite coatings with different nano-Al_2O_3 content

were all hydrophobic, and the contact angle increased with the increase of the nano-Al_2O_3 content. When the nano-Al_2O_3 content was 5 g/L, the contact angle was 151.6°, and the surface was superhydrophobic. When the addition amount of nano-Al_2O_3 was 15 g/L, the contact angle was the maximum, reaching 158.3°, which was corresponding to the results of micromorphology.

Fig. 7 shows the screen captures of the contact angle of the nano-Ni-P-Al_2O_3 (15 g/L) coating. The droplet gradually changed from a sphere to an ellipsoid in the process of the droplet moving down. The droplet gradually changed from a sphere to a spindle shape in the upward movement of the needle, and then returned to a sphere after leaving the coating surface. This indicated that the surface adhesion of the composite coating prepared by electrodeposition and modification was low. There are two classical models for the relationship between rough surface and wettability: Wenzel model [44] and Cassie-Baxter model based on Young's equation [45]. In the Wenzel model, water droplets enter the rough surface and fill the surface. However, the Cassie-Baxter model assumes that the air is captured by the rough surface structure below the water drop, and stays on the rough surface to form an air cushion. The contact interface between the water droplet and the rough structure is a composite interface composed of the liquid-solid interface and liquid-gas interface, and the water droplets are suspended on the rough surface. According to the SEM results, there were many uniform rough structures on the surface of the coating, and the superhydrophobic mechanism diagram of the composite coating is shown in Fig. 8. The Cassie-Baxter model considers that the rough structure contains cavitation formed by air retention. Due to the combined action of the rough structure steel and cavitation, the contact area between the coating surface and liquid was greatly reduced, and the wettability of the coating was reduced.

3.3 Corrosion resistance of coatings with different nano-Al_2O_3 content

Fig. 9 shows the EIS of X100 pipeline steel in the simulated soil solution under different surface states.

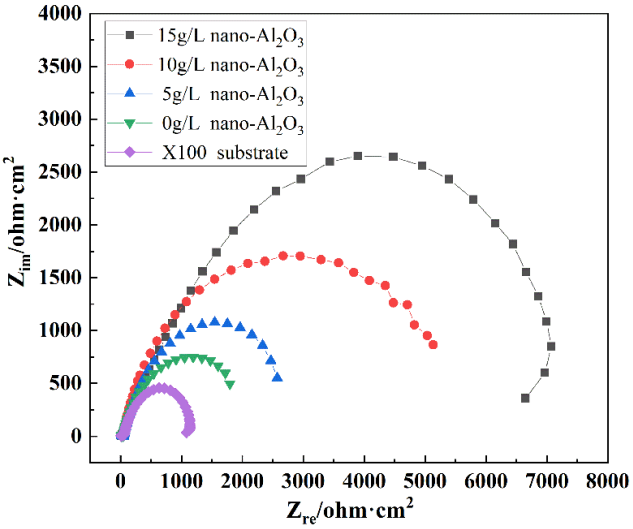

Figure 9. EIS of X100 Pipeline Steel with different surface states in simulated soil solution.

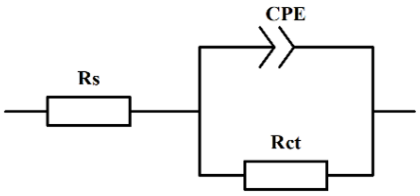

Figure 10. Equivalent circuit model for EIS fitting**.**

The equivalent circuit diagram shown in Fig. 10 is used for fitting, and the fitting results are shown in Table 3, where Rs represents the solution resistance, CPE refers to the constant phase angle, and Rct represents the electrochemical process mass transfer resistance.

Table 3. Fitting results of EIS of different composite coatings on the surface of X100 Pipeline Steel in simulated soil solution.

	R_s ($\Omega \cdot cm^2$)	CPE ($S \cdot s^n \cdot cm^{-2}$)	n	R_{ct} ($\Omega \cdot cm^2$)
X100 substrate	46.575	3.3943×10^{-4}	0.78342	1207.3
0 g/L nano-Al_2O_3	45.593	4.6973×10^{-4}	0.79748	1985.8
5 g/L nano-Al_2O_3	46.356	6.6993×10^{-4}	0.77287	3054.1
10 g/L nano-Al_2O_3	37.808	$6..7415\times10^{-5}$	0.77736	5134.9
15 g/L nano-Al_2O_3	26.409	6.692×10^{-5}	0.68977	8204.4

The dosage of nano-Al_2O_3 did not change the shape characteristics of EIS of the coating, as shown in Fig. 9. The electrochemical impedance spectra of all composite coatings showed a single reactive arc, including reactive arc in the high-frequency region and reactive arc in the low-frequency region. There was no reactive arc in the range of 0-15 g/L at the concentration of nano-Al_2O_3. The radius of the capacitive reactance arc increased gradually with the increase of the nano-Al_2O_3 concentration. The magnitude of capacitive reactance arc represents the magnitude of electrochemical reaction resistance, the larger the capacitive reactance arc is, the greater the electrochemical resistance is, and the better the corrosion resistance is. The content of nano-Al_2O_3 in the plating solution increased from 0 to 15 g/L, and the charge transfer resistance R_{ct} increased from 1891 $\Omega \cdot cm^2$ to 8204.4 $\Omega \cdot cm^2$, both R_s and CPE decreased, and the corrosion rate decreased. Compared with the Ni-P coating and bare X100 pipeline steel, the nano-Ni-P-Al_2O_3 composite coating prepared by adding 15 g/L nano-Al_2O_3 showed a very high impedance value. Nyquist curves of different coatings were fitted into a single semicircle, and the arc radius of the bare X100 pipeline steel was the smallest, that of Ni-P coating was larger, while that of the nano Ni-P-Al_2O_3 composite coating was largest. The results showed that the superhydrophobic Ni-P-Al_2O_3 composite coating had good electrochemical corrosion resistance and excellent corrosion resistance.

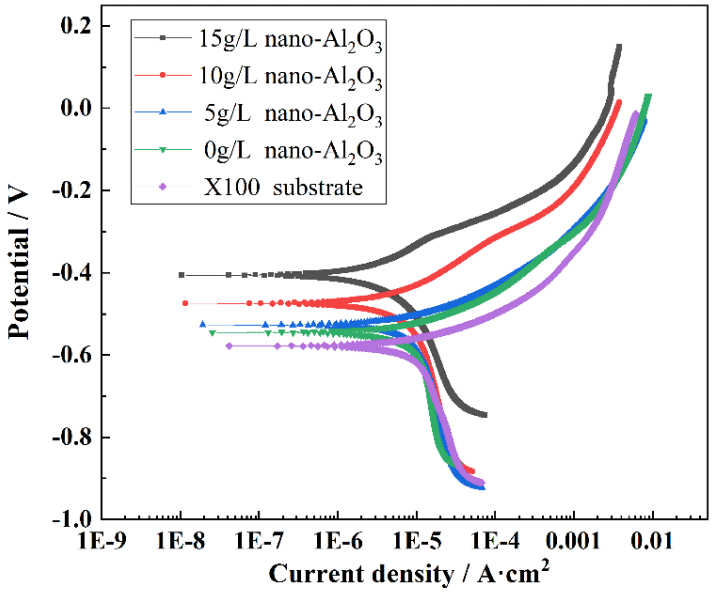

Figure. 11. Potentiodynamic polarization curves of different nano-Al_2O_3 content on X100 pipeline steel in the simulated soil solution.

Fig. 11 shows the polarization curves of different coatings on the X100 pipeline steel surface in the simulated soil solution. The polarization curves were fitted according to the linear extrapolation of Tafel curve. The fitting results are shown in Table 4, E_{corr} represents the self-corrosion potential in the reaction process, and I_{corr} is the self-etching current density in the reaction process.

Table 4. Potentiodynamic polarization curve fitting results of different composite coatings on X100 pipeline steel in the simulated soil solution.

	E_{corr} (V)	I_{corr} (A/cm^2)	Corrosion rate (mm/a)
X100 substrate	-0.578	2.19×10^{-5}	0.257
0 g/L nano-Al_2O_3	-0.545	1.91×10^{-5}	0.224
5 g/L nano-Al_2O_3	-0.527	1.55×10^{-5}	0.182
10 g/L nano-Al_2O_3	-0.474	8.88×10^{-6}	0.104
15 g/L nano-Al_2O_3	-0.405	2.76×10^{-6}	0.032

As shown in Fig. 11, when the addition amount of nano-Al_2O_3 varied from 0-15 g/L, the potentiodynamic polarization curves of the composite coating in the simulated soil solution had similar shapes, indicating that the addition amount of nano-Al_2O_3 had no effect on the electrokinetic polarization curve and the anode and cathode reaction mechanism of the coating. In combination with Table 4, the coating with nano-Al_2O_3 added had higher E_{corr} than the coating without nano-Al_2O_3 added. With the addition of nano-Al_2O_3 increasing from 0 g/L to 15 g/L, E_{corr} increased from -0.545 V to -0.405 V, I_{corr}

decreased continuously, and the corrosion rate also decreased. Compared with the bare X100 pipeline steel substrate (E_{corr}=-0.578 V, I_{corr}=2.19×10^{-5} A/cm^2), the E_{corr} of Ni-P coating increased and I_{corr} decreased. The I_{corr} of the nano-Ni-P-Al_2O_3 composite coating was 2.76×10^{-6} A/cm^2, and the corrosion current decreased, indicating that the corrosion resistance of the coating increased with the addition of nano-Al_2O_3. The E_{corr} (-0.405 V) of nano-Ni-P-Al_2O_3 composite coating was 0.172 V higher than that of bare X100 pipeline steel matrix, which indicated that nano-Al_2O_3 coating had good corrosion resistance.

The microstructure of the composite coating changed greatly as the concentration of the nano-Al_2O_3 particles increased. When nano-Al_2O_3 was added to the Ni-P bath, Ni, P, and nano-Al_2O_3 were easily deposited together, which was attributed to the microstructure of nano-Al_2O_3 providing a core for the deposition of Ni and P [12]. The addition of nano-Al_2O_3 can promote the deposition of Ni and P [45]. The surface grain size of the coating was smaller and more uniform, and the rough structure of the micro-nano level was formed. Due to the irregular pit structure on the surface of the coating, the air was retained in the coating, forming an effective "air cushion" protective layer on the surface. The coating surface had hydrophobic ability after modification with stearic acid solution, making it difficult for the corrosion solution to contact the X100 pipeline steel substrate. At the same time, Al_2O_3 particles are neutral and non-metallic, similar to Cr, TiO_2, SiC, and other particles, the uniform distribution of the nano-Al_2O_3 particles in the coating acted as a "physical barrier" to protect X100 pipeline steel matrix.

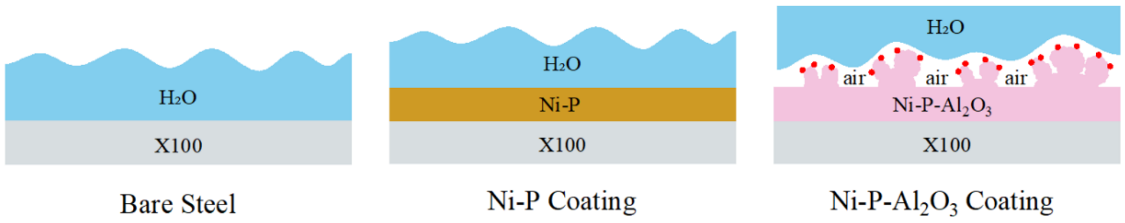

Figure 12. Corrosion diagram of different coatings on the surface of X100 Pipeline Steel.

The corrosion schematic diagram of different coatings on the surface of X100 pipeline steel is shown in Fig. 12. The surface free energy of X100 pipeline steel is large, which made it easier to contact with corrosive media. In addition, the lack of coating protection on the X100 pipeline steel surface led to a large area where corrosion occurred and a high possibility of corrosion. When there was ordinary Ni coating on the surface of X100 pipeline steel, the contact between the X100 pipeline steel and the corrosive medium was reduced. However, the high surface free energy still led to the contact between the corrosive medium and the ordinary Ni coating, which inevitably resulted in the corrosion of the coating and the occurrence of pipeline corrosion. The superhydrophobic coating on the surface of X100 pipeline steel not only reduced the contact between the X100 steel and corrosive medium, but also the contact area between the coating and corrosion medium, thus greatly enhancing the anti-corrosion properties of pipeline steel.

4. CONCLUSIONS

In this study, Ni-P-Al_2O_3 composite coating with micro-nano rough structure was prepared on the surface of X100 pipeline steel by conventional direct current electrodeposition method. The Ni-P-Al_2O_3 composite coating had a superhydrophobic property after modification with a low surface energy material. The microstructure of the coating was changed by changing the amount of the nano-Al_2O_3 particles, and the coating with nano-Al_2O_3 particles grew a mastoid protrude. The coating with 15 g/L nano-Al_2O_3 particles had a uniform and dense surface without obvious holes, the Guglielmi model was used to describe the co-deposition behavior. The hydrophobicity of the coating gradually increased with the addition of nano-Al_2O_3 particles from 0 to 15 g/L. When the nano-Al_2O_3 concentration is 15 g/L, the hydrophobicity of the coating was the best, and the contact angle was 158.3°. The corrosion resistance of the composite coating increased with the increase of the nano-Al_2O_3 concentration. The coating mixed with 15 g/L nano-Al_2O_3 particles had the best corrosion resistance, and the corrosion rate is 0.032731 mm/a. Compared with the naked X100 pipeline steel (0.25746 mm/a), the corrosion rate was greatly reduced and the corrosion resistance was improved.

ACKNOWLEDGEMENTS
Authors would like to thank the Shaanxi Province for Joint fund project (project 2019JLM-45).

References

1. A.O. Ijaola, P.K. Farayibi, E. Asmatulu, *J Nat Gas Sci Eng*., 83 (2020) 103544.
2. L.T. Popoola, A.S. Grema, G.K. Latinwo, *Int.J.Ind*., 4 (2013) 1.
3. J.D. Brassard, D.K. Sarkar, J. Perron, A. Audibert-Hayet, D.Melot, *J. Colloid Interface Sci*., 447 (2015) 240
4. H. Zhang, L. Yin, S. Shi, X. Liu, Y. Wang, *Microelectron. Eng.,* 141 (2015) 238
5. H. Li, S. Yu, X. Han, Y. Zhao, *Colloids Surf. A.*, 503 (2016) 43.
6. M. Askari, M. Aliofkhazraei, S. Afroukhteh, *J Nat Gas Sci Eng.*, 71 (2019).
7. M. Ferrari, A. Benedetti, F. Cirisano, *Coatings*, 9 (2019).
8. D. Yu, J. Tian, J. Dai, X. Wang, *Electrochim. Acta*, 97 (2013) 409.
9. C. Cai, N. Sang, S. Teng, Z. Shen, J. Guo, *Surf. Coat. Technol.*, 307 (2016) 366.
10. Z. Huang, R.S. Gurney, T. Wang, D. Liu, *J. Colloid Interface Sci.*, 527 (2018) 107.
11. Y. Tuo, W. Chen, H. Zhang, P. Li, X. Liu, *Appl. Surf. Sci.*, 446 (2018) 230.
12. T. Chen, S. Ge, H. Liu, Q. Sun, W. Zhu, *Appl. Surf. Sci.*, 356 (2015) 81.
13. G. Wang, T.Y. Zhang, *ACS Appl. Mater. Inter.*, 4 (2012) 273.
14. M. Ramezani, M.R. Vaezi, A. Kazemzadeh, *Appl. Surf. Sci.*, 317 (2014) 147.
15. Y. Liu, J. Liu, S. Li, Y. Wang, Z. Han, L. Ren, *Colloids Surf. A.,* 466 (2015) 125.
16. H.C. Barshilia, N. Gupta, *Vacuum.*, 99 (2014) 42.
17. Z. Yuan, X. Wang, J. Bin, C. Peng, S. Xing, *Appl. Surf. Sci.*, 285 (2013) 205.
18. M. Barahman, A.M. Lyons, *Langmuir,* 27 (2011) 9902.
19. V.S. Kathavate, D.N. Pawar, N.S. Bagal, P.P. Deshpande, *J. Alloys Compd.*, 823 (2020).
20. L. Shen, M. Fan, M. Qiu, W. Jiang, Z. Wang, *Appl. Surf. Sci.* 483 (2019) 706.
21. F. Ebrahimi, H. Li, *Scripta Mater.*, 55 (2006) 263.
22. L. Wang, Y. Gao, Q. Xue, H. Liu, T. Xu, *Appl. Surf. Sci.*, 242 (2005) 326.
23. K.-L. Lin, C.-J. Hsu, I. Hsu, J.-T. Chang, *J.Mater. Eng. Perform.*, 1 (1992) 359.

24. C. Sun, X. Liu, C. Zhou, C. Wang, H. Cao, *Ceram. Int.* 45 (2019) 1348.
25. Y.B. Zhou, J.F. Sun, S.C. Wang, H.J. Zhang, *Corros. Sci*. 63 (2012) 351.
26. M.H. Sarafrazi, M. Alizadeh, *J. Alloys Compd.* 720 (2017) 289.
27. L. Shi, C.F. Sun, F. Zhou, W.M. Liu, Mater. *Sci. Eng. A.*, 397 (2005) 190.
28. X. Peng, T. Li, W. Wu, W. Pan, Mater. *Sci. Eng. A.* 298 (2001) 100.
29. R.K. Saha, T.I. Khan, *Surf. Coat. Technol.*, 205 (2010) 890.
30. X. Zhou, C. Ouyang, *Appl. Surf. Sci.*, 405 (2017) 476.
31. F. Cai, X. Cai, S. Zhang, C. Jiang, *J. Alloys. Compd.*, 738 (2018) 72.
32. S. Chhangani, M.J.N.V. Prasad, *Mater. Charact.*, 136 (2018) 247.
33. R.R. Oberle, M.R. Scanlon, R.C. Cammarata, *Appl. Phys. Lett.*, 66 (1995) 19.
34. S. Ghanbari, F. Mahboubi, *Mater. Des.*, 32 (2011) 1859.
35. F. Cai, C. Jiang, *Appl. Surf. Sci.*, 292 (2014) 620.
36. K. Prevedouros, I.T. Cousins, R.C. Buck, S.H. Korzeniowki, *Environ. Sci. technol.*, 40 (2006) 32.
37. L. Liu, W. Liu, R. Chen, X. Li, X. Xie, *Chem. Eng. J.*, 281 (2015) 804-812.
38. N. Guglielmi, *J. Electrochem. Soc.*, 119 (1972) 1009.
39. J.-P. Celis, J. Roos, C. Buelens, *J. Electrochem. Soc.*, 134 (1987) 1402.
40. J. Fransaer, J.-P. Celis, J. Roos, *J. Electrochem. Soc.*, 139 (1992) 413.
41. Y. Zhao, L. Wang, Y. Sun, H. Liu, C. Jiang, *J. Alloys. Compd.*, 793 (2019) 314.
42. A. Góral, *Surf. Coat. Technol.*, 319 (2017) 23.
43. H.S. Maharana, B. Bishoyi, A. Basu, *J. Alloys. Compd.*, 787 (2019) 483.
44. R.N. Wenzel, *Ind. Eng. Chem.*, 28 (1936) 988.
45. A.B.D. Cassie, S. Baxter, *Trans. Faraday Soc.*, 40 (1944).